[Supplementary Materials]
Inelastic X-ray Scattering for Discrimination of Pigments

Lauren Dalecky, Francesco Sottile, Linda Hung, Laure Cazals, Agnès Desolneux, Aurélia Chevalier, Jean-Pascal Rueff, Loïc Bertrand

Contents

S1 Manufacturer and chemical information of commercial pigments

Laverdure pigments and Sennelier pigments were purchased in September 2021 from their respective boutiques in Paris, France.

Detail on the analysis of the pigments is indicated in Tab. S1.1.

Table S1.1: Manufacturer information, and elemental and structural analysis for all pigments. SDS: Safety Data Sheet, JCPDS: Joint Committee on Powder Diffraction Standards.

Sample	Manufacturer	Commercial designation	SDS information	Pigment elements [trace elements] (SEM-EDX)	Crystal phases [JCPDS] (XRPD)	Density (g/cm^3)
1 La-TiW-r	Laverdure	Blanc de Titane	TiO_2, dioxyde de titane rutile	Ti, O [C, Al, Si, P, S, Zn]	Titanium Oxide Rutile, syn [01-079-6031]	3.75–4.2
2 S-LT	Sennelier	Turquoise Clair (Light Turquoise)	PB28	Ti, O, Co, Al [C, Na, Si, P, K]	Unidentified, found entries similar to Fe_3O_4	4.5
3 La-ZnW	Laverdure	Blanc de Zinc	Oxyde de Zinc ZnO	Zn, O [C, Al, Si]	Zinc oxide ZnO [04-013-6608], [04-013-6608]	5.47-5.65
4 La-VBk	Laverdure	Noir de Vigne	Fe_2O_3, SiO_2, CaO, MgO, Al_2O_3	Fe, O, Ca, Si, Al, Mg [C, Na, S, Cl, P, K, Ti, Mn]	Silicon Oxide SiO_2 [01-078-1256], Iron Oxide Magnetite $Fe_{2.897}O_4$ [01-086-1343], Iron Oxide Hematite syn Fe_2O_3 [04-002-7501]	4.2-5.3
5 La-MBk	Laverdure	Noir de Mars	Fe_2O_3, SiO_2, Al_2O_3, CaO	Fe, O, Si, Al [C, Mg, Na, S, Cl, P, Ca, K, Ti, Mn, Cr]	Silicon Oxide Quartz, syn SiO_2 [01-087-2096], Iron Oxide Magnetite Fe_3O_4 [01-088-0866]	4.2-5.3
6 La-BU	Laverdure	Terre Ombre Brûlée	Fe_2O_3, silice, argile	Fe, O [C, Na, Mg, Al, Si, P, S, K, Ca, Ti]	Silicon Oxide Quartz SiO_2 [04-012-0490], Iron Titanium Oxide Hematite, Ti-bearing $(Fe_{1.831}Ti_{0.169})O_3$ [01-079-5903], Iron Oxide Magnetite Fe_3O_4 [01-080-6402], Iron Oxide Hematite, syn Fe_2O_3 [04-015-6943]	4.2-5.3
7 La-PB	Laverdure	Bleu de Prusse	CAS 25869-0051	Fe, C [O, Na, Al, Si, S, Cl, Ca, Ti, Zn]	Prussian blue $Fe_7C_{18}N_{18}$ [00-052-1907]	1.83

Continued on next page

3

Table S1.1: Manufacturer information, and elemental and structural analysis for all pigments. SDS: Safety Data Sheet, JCPDS: Joint Committee on Powder Diffraction Standards. (Continued)

Sample	Manufacturer	Commercial designation	SDS information	Pigment elements [trace elements] (SEM-EDX)	Crystal phases [JCPDS] (XRPD)	Density (g/cm^3)
8 La-IBk	Laverdure	Noir d'Ivoire	CALCIUM PHOSPHATE + CARBONE	Ca, C, O, P [Na, Mg, Al, Si, S, Cl, Ca]	Calcium Phosphate Hydroxide Hydroxylapatite Ca$_5$(PO$_4$)$_3$(OH) [01-073-8419]	2.29
9 La-UB	Laverdure	Bleu Outremer	Aluminosilicate de sodium polysulfuré, Pigment bleu 29, Carbonate de calcium	Na, Al, Si, S, Ca, C, O [Mg, P, K, Fe]	Lazurite Na$_{3.12}$Al$_{2.97}$Ca$_{0.8}$Mg$_{0.36}$O$_{15.12}$SSi$_{3.03}$ [96-901-1356], Huayne Na$_6$Ca$_2$(Al$_6$Si$_6$O$_{24}$)(SO$_4$)$_2$ [96-154-1699], Calcium Magnesium Carbonate Dolomite CaMg(CO$_3$)$_2$ [96-900-3509], Calcite Ca(CO$_3$) [96-901-1356]	2.34
10 La-IYI	Laverdure	Jaune Indien Imitation	Pigment Yellow 150 Nickel, 5,5-azobis-2,4,6(1H,3H,5H)-pyrimidinetrione complexes and melamine	Ni, C, N, O [Na, Cl]	Unidentified, amorphous	2.0-2.1
11 S-QR	Sennelier	Rouge de Quinacridone (Quinacridone Red)	PR122	C, O [C, Na, Mg, Al, Si, P, S, Ca]	2,9-Dimethylquinacridone C$_{22}$H$_{16}$N$_2$O$_2$ [00-039-1876]	1.5
12 S-TiW-a	Sennelier	Blanc de Titane (Titanium White)	Dioxyde de titane	Ti, O [C, Al, Si, P, K]	Titanium Oxide Anatase, syn [04-014-5762] (97.7%), Titanium Oxide Rutile, syn [01-086-4329] (2.3%)	3.7–3.9
13 CQ-TiW-a	Couleurs du Quai	Blanc de Titane (Titanium White)	—	Ti, O [C, Al, Si, P, K]	Titanium Oxide Anatase, syn [04-014-5764] (98.5%) Titanium Oxide Rutile, syn [01-079-5859] (1.5%)	3.7–3.9

4

Table S1.1: Manufacturer information, and elemental and structural analysis for all pigments. SDS: Safety Data Sheet, JCPDS: Joint Committee on Powder Diffraction Standards. (Continued)

Sample	Manufacturer	Commercial designation	SDS information	Pigment elements [trace elements] (SEM-EDX)	Crystal phases [JCPDS] (XRPD)	Density (g/cm^3)
14 F-TiW-r	Fitzpatrick	Titanium White	PW6	Ti, O [C, Si, Al, Zn, Mg, Cl]	Titanium Oxide Rutile, syn [04-005-4625]	3.75–4.2
15 K-TiW-r	Kremer	Titanium White	rutile	Ti, O [C, Al, Si, Zn]	Titanium Oxide Rutile, syn [01-079-6031] (90.5%) Titanium Oxide Anatase, syn [01-070-6826] (9.5%)	3.75–4.2
16 X-R-r	N/A	"Rutile"	—	Ti, O [C, Al, Si, Zn, Ca, P, S]	Titanium Oxide Rutile, syn [04-005-4625] (99.2%) Titanium Oxide Anatase, syn [00-064-0863] (0.8%)	3.75–4.2

S2 Experimental configurations

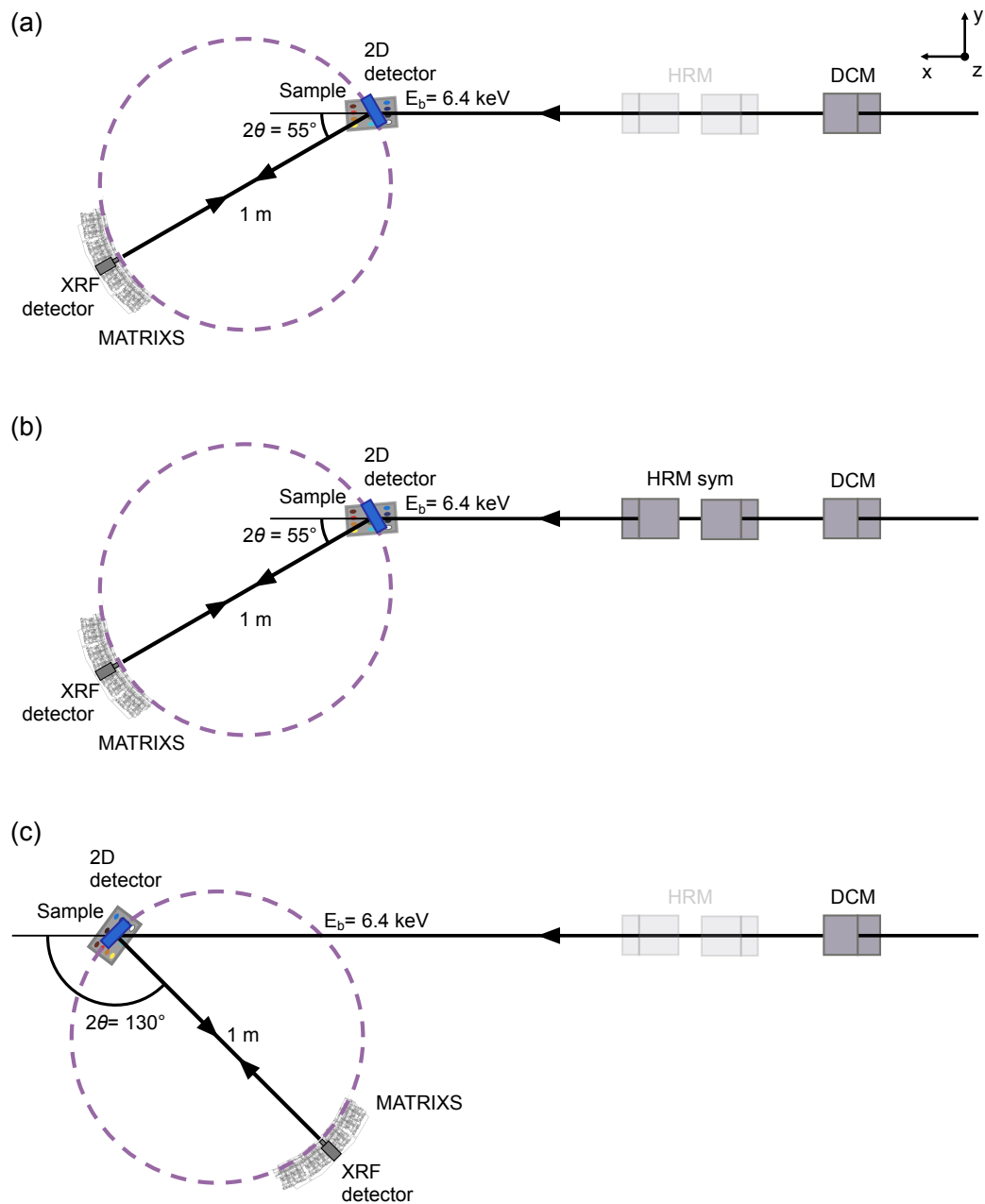Three experimental configurations were used (Fig. S2.1 and Tab. S2.1).

Figure S2.1: Schematic representation of the three configurations used at the GALAXIES beamline: forward scattering in low resolution (a) and high resolution (b) modes, and back scattering in low resolution mode (c).

Table S2.1: Additional information regarding the irradiation parameters for each of the three configurations. Config.: configuration; Mono.: monochromator(s).

Config.	Mono.	Flux (ph/s)	Count time (s)	Dead time (%)	Live time (s)	Beam area (μm^2)	Fluence (ph/μm^2)
Fig. S2.1(1)	DCM	3×10^{13}	1184	59%	1884	3000	1.9×10^{13}
Fig. S2.1(2)	DCM; HRM	5×10^{12}	4000	7.0%	4287	3000	7.2×10^{12}
Fig. S2.1(3)	DCM	3×10^{13}	3.0	73%	5.2	3000	5.2×10^{10}

S3 Additional experimental and simulated DSF spectra for the anatase and rutile-based pigments
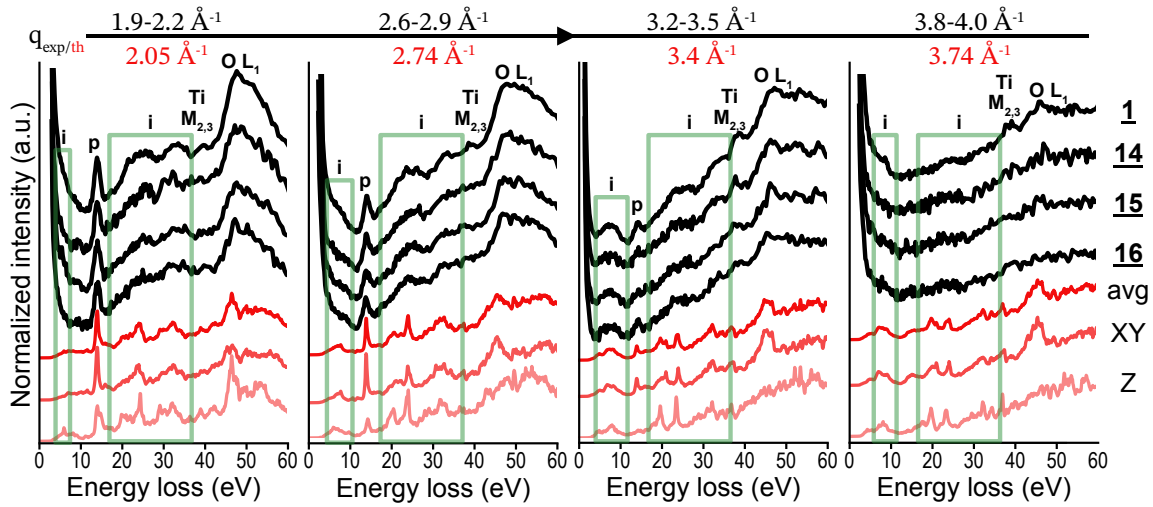

Figure S3.1: Experimental spectra (black) of rutile-based pigments at low energy transitions (energy resolution: 800 meV) and corresponding DSF calculations (red) of rutile averaged in the XY and Z planar directions, XY direction only, and Z direction only.
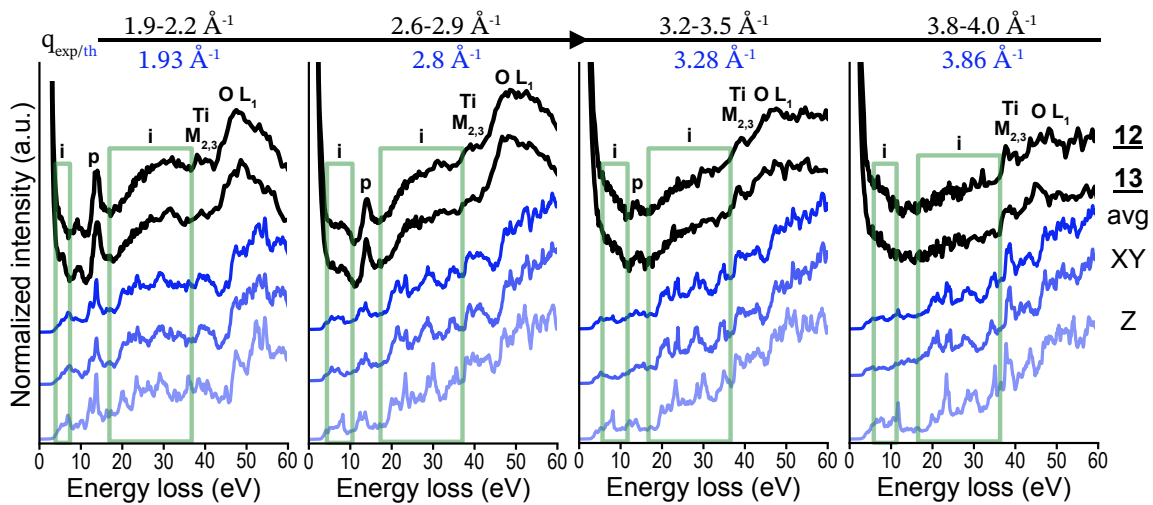

Figure S3.2: Experimental spectra of anatase-based (black) pigments at low energy transitions (energy resolution 800 meV) and corresponding DSF calculations (blue) of anatase averaged in the XY and Z planar directions, XY direction only, and Z direction only.
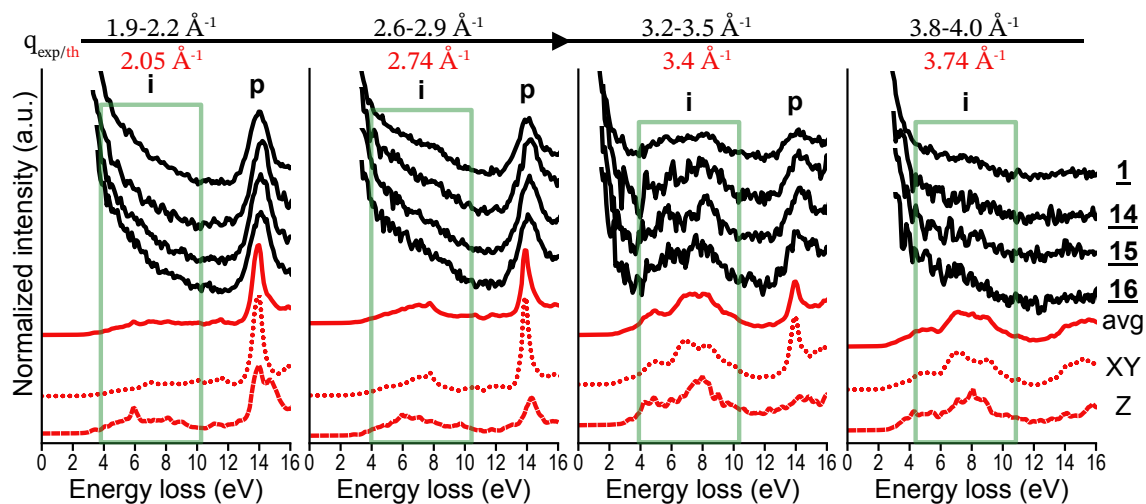
Figure S3.3: Experimental spectra (black) of rutile-based pigments at the plasmon resonance (energy resolution 300 meV) and corresponding DSF calculations (red) of rutile averaged in the XY and Z planar directions, XY direction only, and Z direction only.
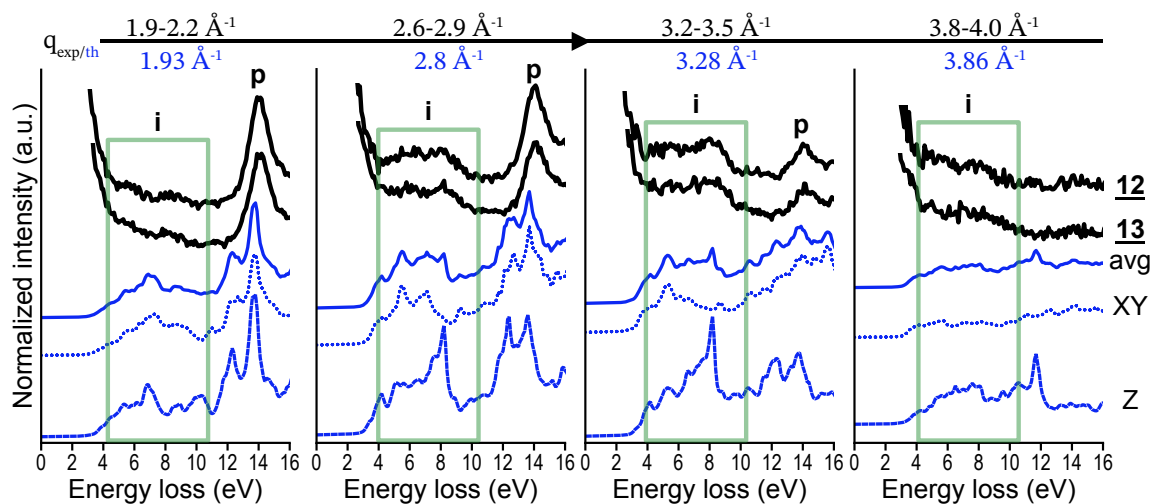

Figure S3.4: Experimental spectra (black) of anatase-based pigments at the plasmon resonance (energy resolution 300 meV) and corresponding DSF calculations (blue) of anatase averaged in the XY and Z planar directions, XY direction only, and Z direction only.

S4 Anisotropy of rutile and anatase

As depicted in Fig. S4.1, while the two tetragonal structures present a clear anisotropy, the difference between the X and Z directions is not very high. It is slightly bigger in rutile (bottom panel) than in anatase (top panel).
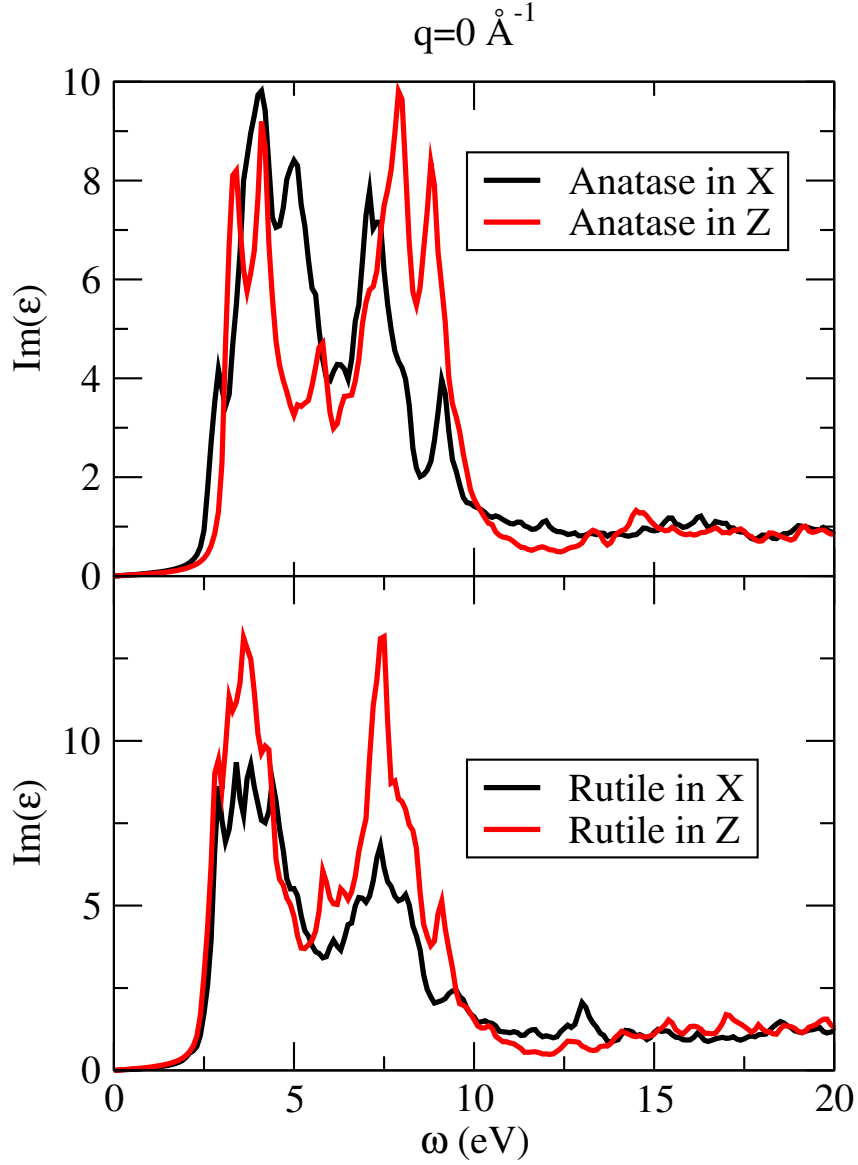

Figure S4.1: Imaginary part of the dielectric function at vanishing momentum transfer for the two equivalent directions (X is represented by the black curves, while direction Z is depicted via the red curves).

S5 Theoretical approach

We describe here the framework in which the numerical calculations have been conducted. The dynamical structure factor can be related to the inverse dielectric function

$$S(\mathbf{q}, \omega) = -\frac{\hbar^2 q^2}{4\pi^2 e^2 n} \mathrm{Im}(\varepsilon^{-1}(\mathbf{q}, \omega)) \tag{1}$$

and, in turn, directly to the macroscopic dielectric function ε (which is related, among other things, to optical properties)

$$S(\mathbf{q}, \omega) = \frac{\hbar^2 q^2}{4\pi^2 e^2 n} \frac{\mathrm{Im}[\varepsilon(\mathbf{q}, \omega)]}{\mathrm{Re}[\varepsilon(\mathbf{q}, \omega)]^2 + \mathrm{Im}[\varepsilon(\mathbf{q}, \omega)]^2} \tag{2}$$

similarly to what is done for the Electron Energy Loss function [11]. Here, n, e, $\hbar$ are the average electron density, the electron charge and the Planck constant, respectively. The inverse dielectric function has been obtained within the ab initio framework of Time Dependent Density Functional Theory (TDDFT) [3, 4], in the Random Phase Approximation (RPA). In this approach, one starts by performing a ground-state Density Functional Theory calculation [1], using the Kohn-Sham scheme [2], typically within the Local Density Approximation or, like in our case, within the Generalised Gradient Approximation (GGA) [6]. The one-electron eigenvalues and eigenfunctions obtained with this calculation permit, on one hand, a careful analysis of the band structure of the material, and on the other, they permit to build the independent-particle polarizability χ^0 [7], with which the full polarizability χ is evaluated

$$\chi_{\mathbf{G}\mathbf{G}'}(\tilde{\mathbf{q}}, \omega) = \chi^0_{\mathbf{G}\mathbf{G}'}(\tilde{\mathbf{q}}, \omega) + \sum_{\mathbf{G}''} \chi^0_{\mathbf{G}\mathbf{G}''}(\tilde{\mathbf{q}}, \omega) v_{\mathbf{G}''}(\tilde{\mathbf{q}}) \chi_{\mathbf{G}''\mathbf{G}'}(\tilde{\mathbf{q}}, \omega) \tag{3}$$

where $\tilde{\mathbf{q}}$ lies in the first Brillouin zone (BZ), $\mathbf{G}$ is a reciprocal lattice vector, and $v_{\mathbf{G}}(\tilde{\mathbf{q}}) = \frac{4\pi}{|\tilde{\mathbf{q}}+\mathbf{G}|^2}$ is the Coulomb interaction. So, by considering the connection between the inverse dielectric function and the polarizability ($\varepsilon^{-1} = 1 + v\chi$) the DSF for a given momentum transfer $\mathbf{q} = \tilde{\mathbf{q}} + \mathbf{G}$ and energy loss ω, is

$$S(\mathbf{q}, \omega) = -\frac{\hbar^2 q^2}{\pi e^2 n |\tilde{\mathbf{q}}+\mathbf{G}|^2} \mathrm{Im}(\chi_{\mathbf{G}\mathbf{G}}(\tilde{\mathbf{q}}, \omega)) \tag{4}$$

$$\propto -\mathrm{Im}(\chi_{\mathbf{G}\mathbf{G}}(\tilde{\mathbf{q}}, \omega)). \tag{5}$$

For the specific case of vanishing momentum transfer $\mathbf{q}$ (or, in general, for a momentum transfer smaller than the first BZ), Eq. (5) becomes

$$S(\mathbf{q}, \omega) \propto -\mathrm{Im}(\chi_{00}(\mathbf{q}, \omega)). \tag{6}$$

S6 Computational details of the numerical calculations of TiO$_2$

Rutile and anatase TiO$_2$ belong to the P4mmm and I4amd spatial groups, respectively. We have calculated, within DFT and using the GGA-PBE approximation[6], the lattice constants, which are $a = 4.64$ Å, $c = 2.96$ Å for rutile and $a = 3.80$ Å, $c = 9.70$ Å for anatase, i.e. within 3% of the experimental values. The norm-conserving Troullier-Martins [5] pseudopotentials for Titanium and Oxygen are also evaluated within GGA-PBE. Ground-state calculations have been performed with the Abinit package [9], using an energy cutoff of 100 Hartree (both structures) and 12 and 9 k-points in the irreducible Brillouin Zone (BZ), for anatase and rutile, respectively. The dielectric functions and DSF have been evaluated with the DP code [12], using 144 shifted k-points in the full BZ [8], 24 occupied bands (that corresponds to the 48 electrons present in both structures) and 126 empty bands. We have used 3807 and 3879 plane waves for the expansions of the wavefunctions (in rutile and anatase, respectively), as well as 245 and 233 (for rutile and anatase, respectively) $\mathbf{G}-$vectors for the inversion of $\chi_{\mathbf{GG'}}$, that permits one to converge the local field effects.

S7 Experimental and calculated IXS spectra in TiO$_2$ crystals

To compare to the numerical calculations, the IXS spectra were measured in TiO$_2$ single crystals for both rutile and anatase phases with **q** aligned along the 100 and 110 directions. The measurements were performed at the GALAXIES beamline using photons energy of 9.7 keV and a total resolution of 1.5 eV. The results are displayed in Fig. S7.1 for q ranging approximately from $1\,\text{Å}^{-1}$ to $5\,\text{Å}^{-1}$ and an energy loss up to 60 eV. The experimental spectra are shown in panels (a) and (b) for rutile and anatase phase respectively with q increasing from bottom to top, while the corresponding calculations are displayed in panels (c) and (d). The calculations correctly reproduces the experimental features and their dispersion.
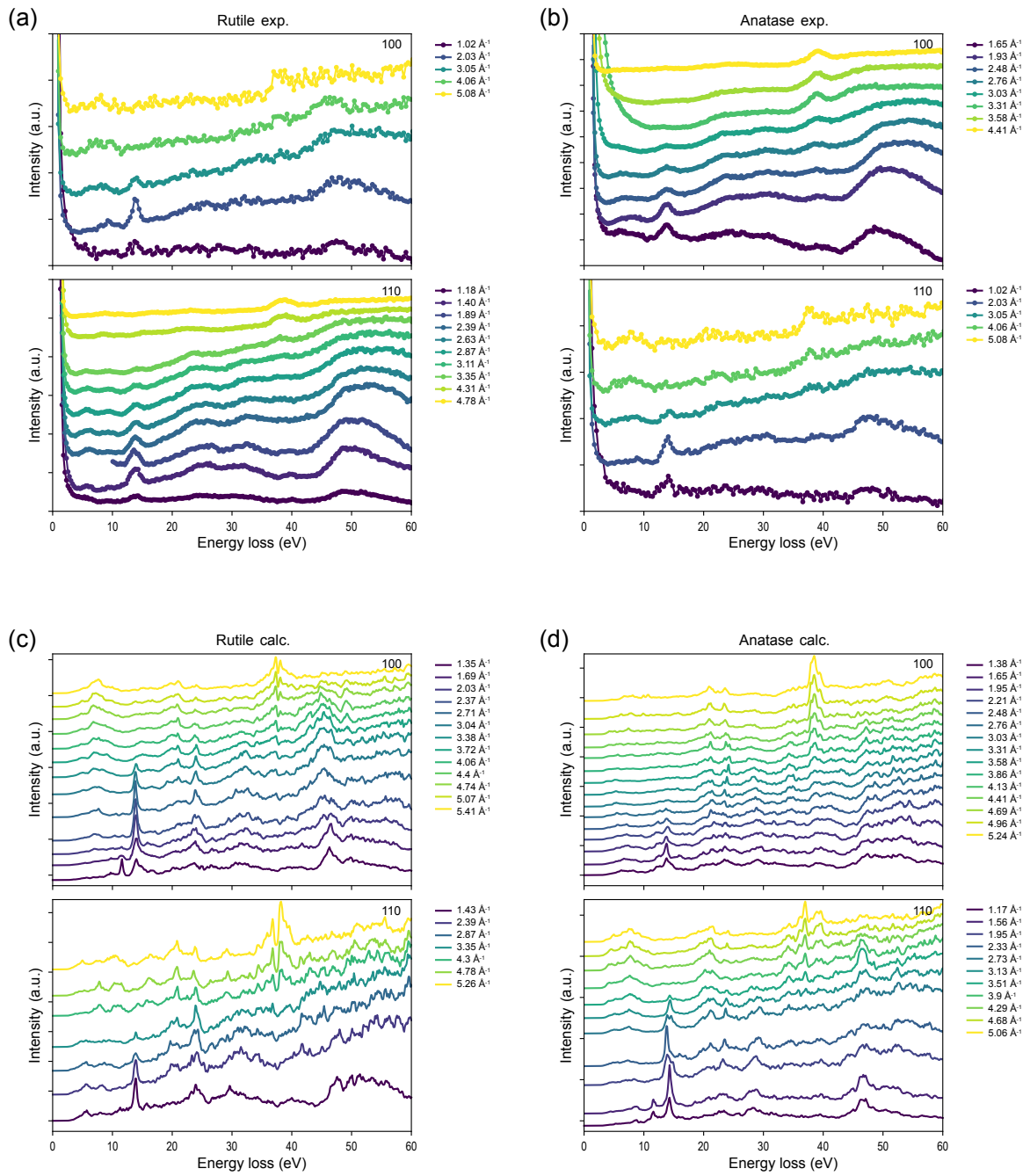
Figure S7.1: IXS spectra in TiO$_2$ rutile and anatase single crystals for **q** aligned along the 100 and 110 directions as a function of the energy loss. The experimental results are summarised in panels (a) and (b) for rutile and anatase phase, respectively, and the calculations in panels (c) and (d).

S8 Dispersion of bulk rutile and anatase along the Z direction

As mentioned briefly in the main text (see Fig. 5), the main peak at around $14\,$eV has been interpreted as a plasmon peak. The definition of the plasmon peak is much more clear at $q = 0$, where it is given by the condition $\mathrm{Re}(\varepsilon) = 0$, immediately after the anomalous dispersion. The black curves at the bottom of both of Fig. S8.1 and Fig. S8.2, for rutile and anatase, respectively, show the DSF and the $\mathrm{Re}(\varepsilon)$ for a very small momentum transfer. The crossing of the $\mathrm{Re}(\varepsilon)$ with the energy axis shows the plasmon, and we can follow its dispersion at increasing momentum transfer (other colors in the figures). It is more difficult to perform this analysis knowing only a spectrum at high momentum transfer because $\mathrm{Re}(\varepsilon)$ tends to be a constant, the DSF becomes equivalent to the $\mathrm{Im}(\varepsilon)$, and the distinction between interband and plasmon becomes very difficult.

At zero momentum transfer the main plasmon peak is at $12\,$eV, to become a double peak structure (12 and $14\,$eV) in both rutile and anatase at small momenta. At high momentum transfer instead, the first peak is smoothed out in rutile, but not in anatase.
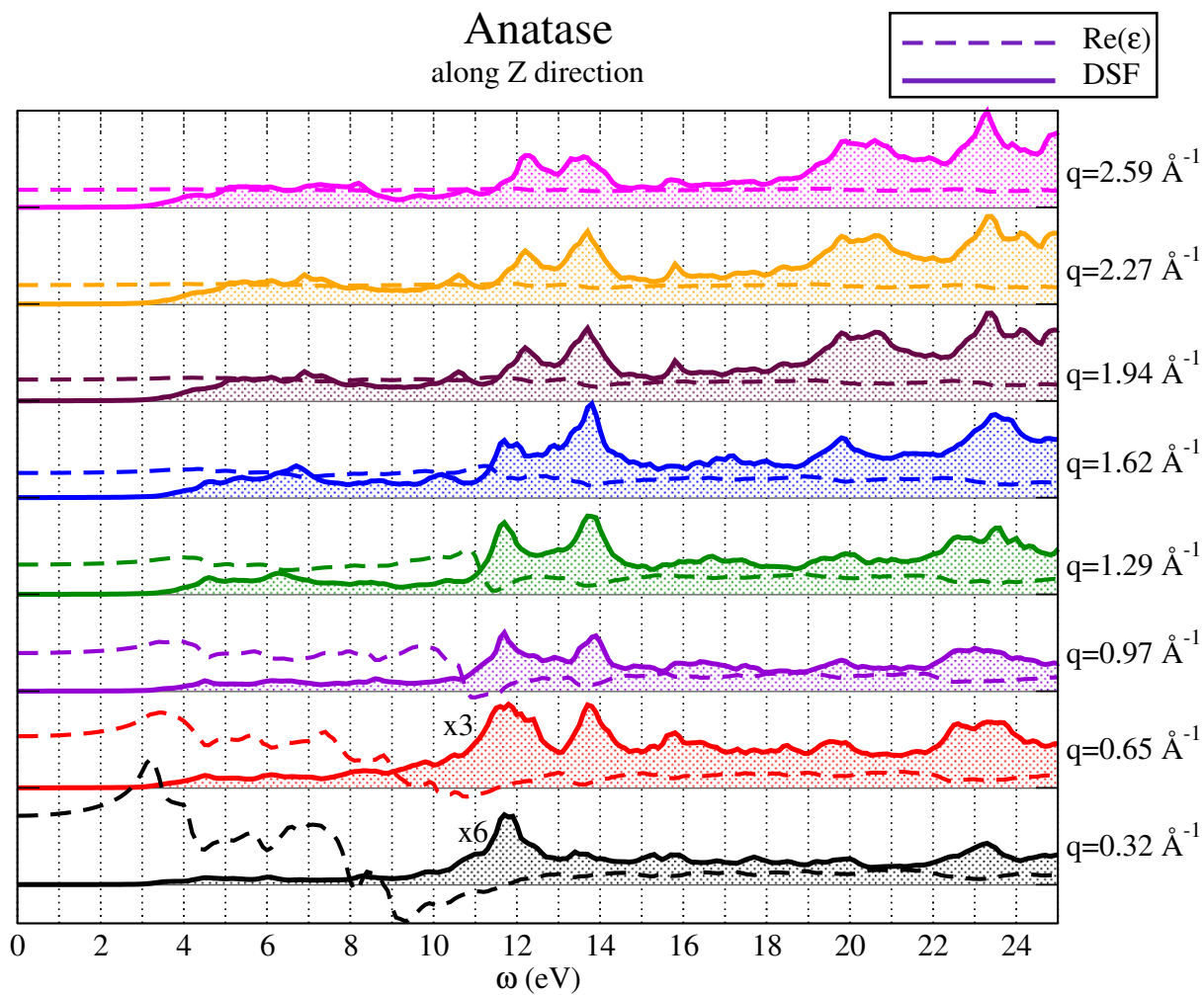
Figure S8.1: DSF of Anatase TiO_2 for different momentum transfer along the Z direction. For an easier analysis, we also report the corresponding real part of the dielectric function (in dashed lines) that shows the plasmonic character of both peaks at 12 and 14 eV.
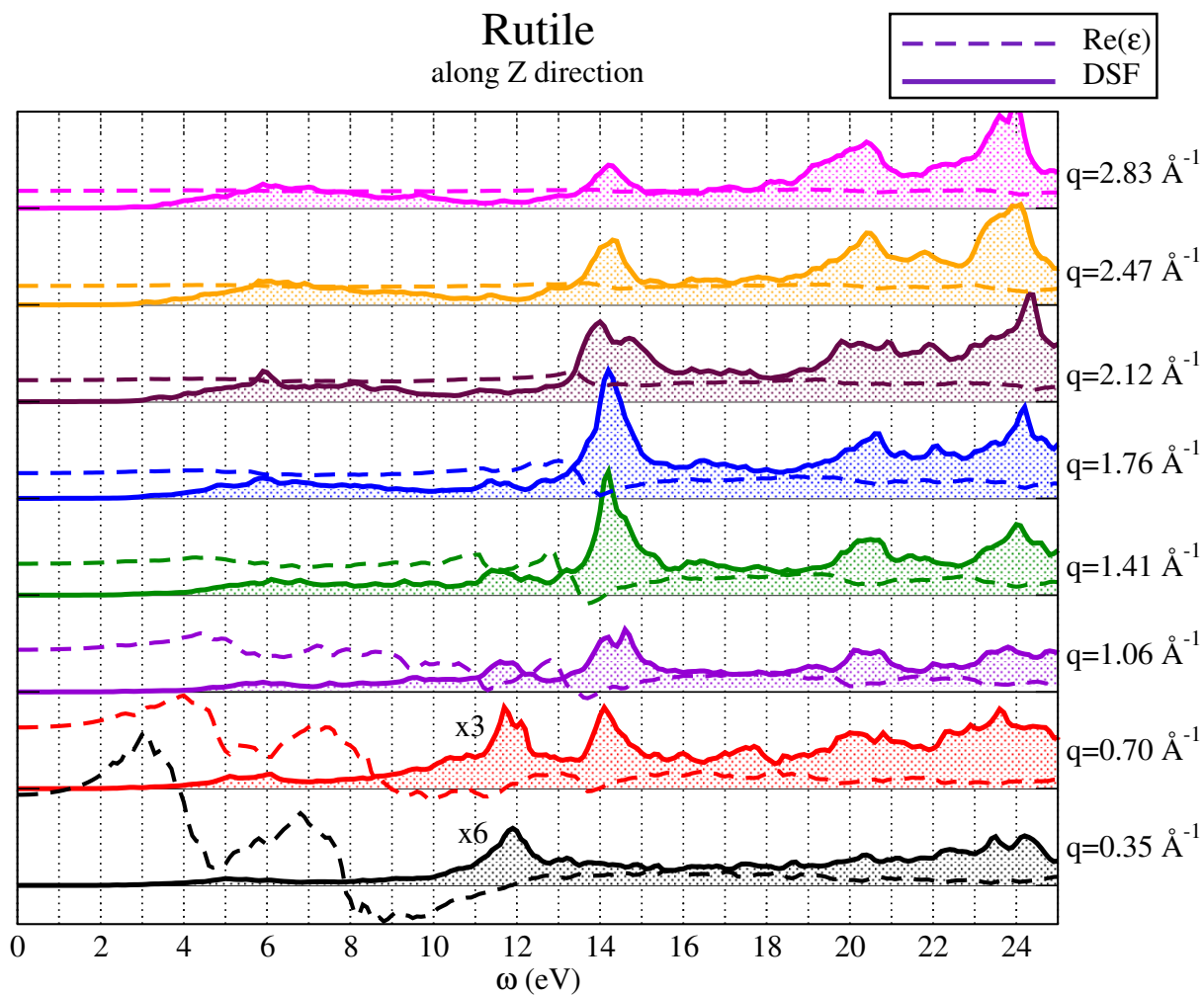
Figure S8.2: DSF of Rutile TiO_2 for different momentum transfer along the Z direction. For an easier analysis, we also report the corresponding real part of the dielectric function (in dashed lines) that shows the plasmonic character of both peaks at 12 and 14 eV.

S9 Comparing experiment with theory and role of local field effects

In spite of the overall good agreement between theory and experiment for the DSF of TiO_2, some discrepancies are present. Most noteworthy is the double plasmon peak (12, 14 eV) of anatase: visible in the calculation, but absent in the experimental results. Here, we must emphasize the difference between an ideal theoretical structure and a real powder sample. The origin of the double peak is illustrated in Fig. S9.1, in which we conduct the analysis on both anatase and rutile. The DSF (black curve of the top panels, for both rutile and anatase) is shown together with the real and imaginary parts of the dielectric function (black curves in central and bottom panels). The peaks and structure of $Im(\varepsilon)$ are related to interband transitions, while the anomalous dispersion in $Re(\varepsilon)$ reveals the plasmon. The latter comes from the collective excitations of the O-2p $\rightarrow$ Ti-3d electrons, whose states constitute the top valence. We can notice, by comparing black and red curves (that correspond to the same quantity of the black curve, but excluding the local field effects, i.e. excluding the sum over $\mathbf{G}''$ in Eq.(3)), that the shift to high energy (and the plasmon formation) of the O-2p excitations is due to the correct treatment of the local fields. This was already pointed out in TiO_2, even at zero momentum transfer [10], but it becomes crucial at high momentum. The effect of the local fields seems to be more important in rutile (with a stronger push at higher energy) than in anatase. The results is that the DSF in anatase is more similar to the $Im(\varepsilon)$ than in rutile, so keeping the multi-peak structure. This effect happens to be stronger in the Z-direction. It is also true that the rutile is slightly more anisotropic than anatase (see Supplementary Fig. S4.1). An obvious consequence is that it is crucial to include local fields, and go beyond a simple sum-over-state approach for the numerical calculations. It is important to underline that the double peak structure in anatase (and also in rutile, at different momentum transfer) is very well present in the experimental spectra of crystal TiO_2: in Fig. S7.1, the full experimental dispersion is shown and compared with the numerical results, showing a very good agreement. The missing double peak in the experiment of the powder is then due to the particular sample. This shows how far from trivial it is to extract meaningful information from the pigment measurements. Only a combined series of approaches (both experimental and theoretical), together with a wide energy and momentum range, can guarantee a reliable and quantitative analysis of the results.
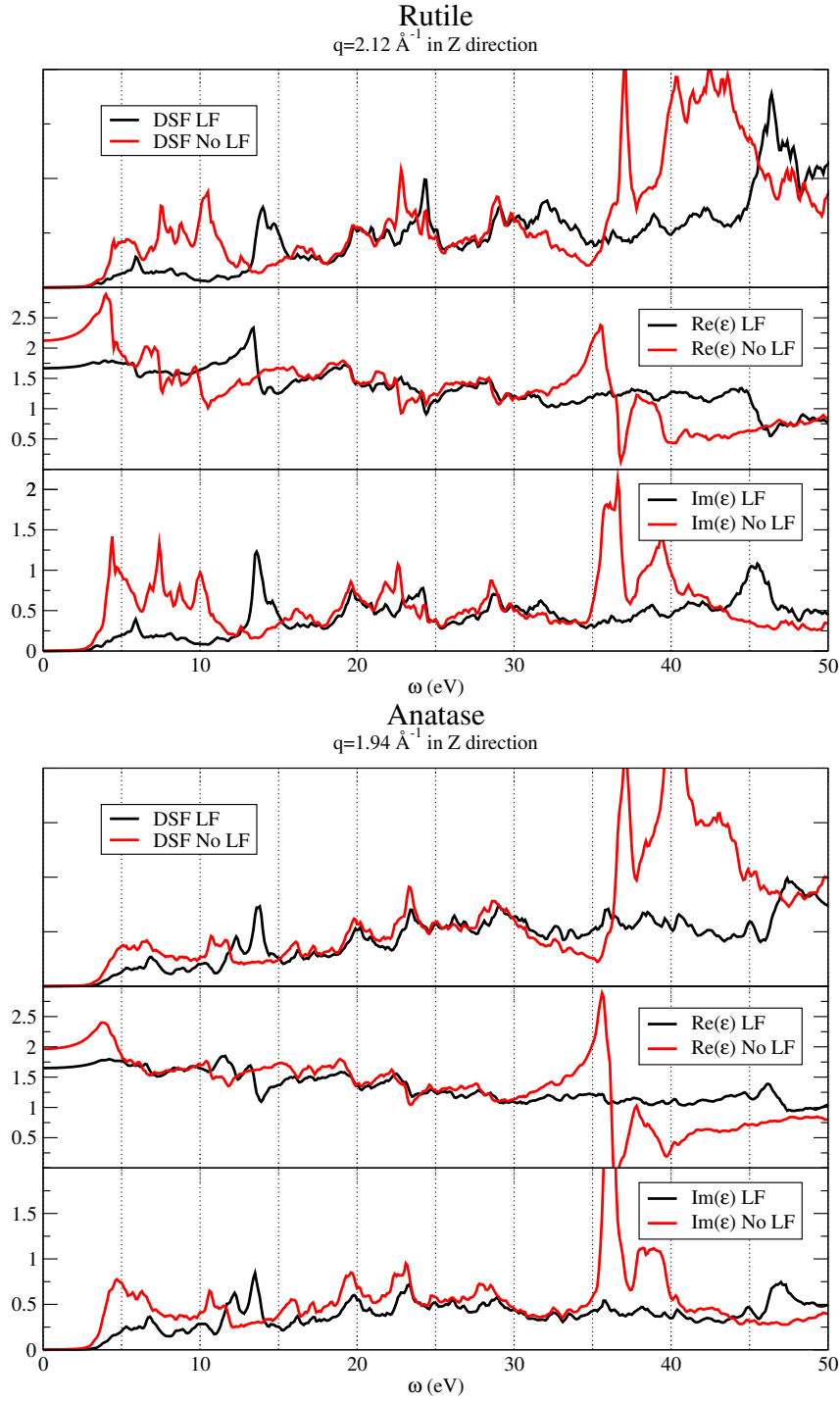
Figure S9.1: For rutile (top image) and anatase (bottom image): effect of the local fields (included in the black curves, neglected in the red curves) in the Real and Imaginary part of the ε, as well as in the DSF. In the Z-direction, the local field effects are stronger in the rutile structure, pushing the plasmon to form a more prominent structure at slightly higher energy. Here ω has the meaning of absorption frequency (for Real and Imaginary part of ε) or of Energy Loss for the DSF. The dielectric function ε is given in absolute units (it is adimensional) while the DSF is given in arbitrary units.

References

[1] P. Hohenberg and W. Kohn. "Inhomogeneous Electron Gas". en. In: *Physical Review* 136.3B (Nov. 1964), B864–B871. ISSN: 0031-899X. DOI: 10.1103/PhysRev.136.B864. URL: https://link.aps.org/doi/10.1103/PhysRev.136.B864 (visited on 13/04/2023).

[2] W. Kohn and L. J. Sham. "Self-Consistent Equations Including Exchange and Correlation Effects". en. In: *Physical Review* 140.4A (Nov. 1965), A1133–A1138. ISSN: 0031-899X. DOI: 10.1103/PhysRev.140.A1133. URL: https://link.aps.org/doi/10.1103/PhysRev.140.A1133 (visited on 13/04/2023).

[3] Erich Runge and E. K. U. Gross. "Density-Functional Theory for Time-Dependent Systems". en. In: *Physical Review Letters* 52.12 (Mar. 1984), pp. 997–1000. ISSN: 0031-9007. DOI: 10.1103/PhysRevLett.52.997. URL: https://link.aps.org/doi/10.1103/PhysRevLett.52.997 (visited on 13/04/2023).

[4] E. K. U. Gross and Walter Kohn. "Local density-functional theory of frequency-dependent linear response". en. In: *Physical Review Letters* 55.26 (Dec. 1985), pp. 2850–2852. ISSN: 0031-9007. DOI: 10.1103/PhysRevLett.55.2850. URL: https://link.aps.org/doi/10.1103/PhysRevLett.55.2850 (visited on 13/04/2023).

[5] N. Troullier and José Luriaas Martins. "Efficient pseudopotentials for plane-wave calculations". en. In: *Physical Review B* 43.3 (Jan. 1991), pp. 1993–2006. ISSN: 0163-1829, 1095-3795. DOI: 10.1103/PhysRevB.43.1993. URL: https://link.aps.org/doi/10.1103/PhysRevB.43.1993 (visited on 23/04/2023).

[6] John P. Perdew, Kieron Burke and Matthias Ernzerhof. "Generalized Gradient Approximation Made Simple". en. In: *Physical Review Letters* 77.18 (Oct. 1996), pp. 3865–3868. ISSN: 0031-9007, 1079-7114. DOI: 10.1103/PhysRevLett.77.3865. URL: https://link.aps.org/doi/10.1103/PhysRevLett.77.3865 (visited on 13/04/2023).

[7] M. Petersilka, U. J. Gossmann and E. K. U. Gross. "Excitation Energies from Time-Dependent Density-Functional Theory". en. In: *Physical Review Letters* 76.8 (Feb. 1996), pp. 1212–1215. ISSN: 0031-9007, 1079-7114. DOI: 10.1103/PhysRevLett.76.1212. URL: https://link.aps.org/doi/10.1103/PhysRevLett.76.1212 (visited on 13/04/2023).

[8] Lorin X. Benedict, Eric L. Shirley and Robert B. Bohn. "Theory of optical absorption in diamond, Si, Ge, and GaAs". en. In: *Physical Review B* 57.16 (Apr. 1998), R9385–R9387. ISSN: 0163-1829, 1095-3795. DOI: 10.1103/PhysRevB.57.R9385. URL: https://link.aps.org/doi/10.1103/PhysRevB.57.R9385 (visited on 21/04/2023).

[9] X. Gonze et al. "First-principles computation of material properties: the ABINIT software project". en. In: *Computational Materials Science* 25.3 (Nov. 2002), pp. 478–492. ISSN: 09270256. DOI: 10.1016/S0927-0256(02)00325-7. URL: https://linkinghub.elsevier.com/retrieve/pii/S0927025602003257 (visited on 21/04/2023).

[10] Nathalie Vast et al. "Local Field Effects in the Electron Energy Loss Spectra of Rutile TiO 2". en. In: *Physical Review Letters* 88.3 (Jan. 2002), p. 037601. ISSN: 0031-9007, 1079-7114. DOI: 10.1103/PhysRevLett.88.037601. URL: https://link.aps.org/doi/10.1103/PhysRevLett.88.037601 (visited on 04/03/2023).

[11] Winfried Schülke. *Electron dynamics by inelastic X-ray scattering*. eng. Oxford series on synchrotron radiation 7. Oxford: Oxford Univ. Press, 2007. ISBN: 978-0-19-851017-8.

[12] V. Olevano, Reining, Lucia and Francisco Sottile. *The DP code, Olevano, V. and Reining, L. and Sottile, F.,* URL: https://etsf.polytechnique.fr/Software/Ab_Initio.